PHYSICAL REVIEW B **78**, 121403(R) (2008)

Intrinsic spin Hall effect in graphene: Numerical calculations in a multiorbital model

Seiichiro Onari,[1] Yasuhito Ishikawa,[1] Hiroshi Kontani,[2] and Jun-ichiro Inoue[1]
[1]*Department of Applied Physics, Nagoya University, Chikusa, Nagoya 464-8603, Japan*
[2]*Department of Physics, Nagoya University, Chikusa, Nagoya 464-8603, Japan*
(Received 12 June 2008; revised manuscript received 20 August 2008; published 11 September 2008)

We study the spin Hall effect (SHE) in graphene using a realistic multiorbital tight-binding model that includes the atomic spin-orbit interaction. The SHE is found to be induced by the spin-dependent Aharonov-Bohm phase. In the metallic case, the calculated values for the spin Hall conductivity (SHC) are much smaller than the quantized Hall conductivity for realistic parameter values of metallic graphene. In the insulating case, quantization of the SHC is violated due to the multiorbital effect. The present study suggests that the SHE in a honeycomb lattice is enhanced by chemical doping, such as the substitution of carbon atoms with boron atoms.

DOI: 10.1103/PhysRevB.78.121403 PACS number(s): 73.43.−f, 72.25.Hg, 73.61.Wp, 85.75.−d

The recent discovery of graphene has stimulated much interest in electron transport in graphene due to its unconventional electronic structure.[1] The crystal structure of graphene is a two-dimensional honeycomb lattice of carbon atoms. In the absence of the spin-orbit interaction (SOI), the band structure of graphene is described in terms of massless Dirac fermions at the edges (K and K' points) of the Brillouin zone. Due to a nonzero Berry's phase (a geometric quantum phase),[2] a striking "half-integer" quantum Hall effect is realized in graphene.[3,4] The nature of the quantum Hall effect near the massless Dirac point has been studied theoretically.[5–10] Concerning transport phenomena in graphene, the emergence of a sizable spin Hall effect (SHE), which is a phenomenon where a spin current flows perpendicular to an applied electric field, had been predicted theoretically.[11,12] In particular, Kane and Mele[11] have demonstrated that the SOI generates an energy gap at the Dirac point, and the "quantum SHE" is expected to appear in insulating graphene.

Recently, the theory of the intrinsic SHE caused by the Berry phase in zincblende semiconductors[13] or by a uniform SOI such as the Rashba SOI in a two-dimensional electron gas[14] has been attracting much interest. Quite recently, the SHE has also been observed in the simple metal Al (Ref. 15) and the transition metal Pt.[16] The spin Hall conductivity (SHC) reported for Pt is $240(\hbar/e)(\Omega\ \mathrm{cm})^{-1}$ at room temperature, which is much larger than that of semiconductors. The huge SHC in Pt has been explained theoretically by Kontani *et al.* in terms of the atomic SOI and a realistic tight-binding (TB) model that includes interorbital hopping integrals.[17–19] They further showed that the so-called current vertex corrections (CVCs) have little effect on the SHC in transition metal, in contrast to that in semiconductors with the Rashba SOI.[20]

The successful reproduction of the experimental values of the SHC in transition metals by the TB model with the atomic SOI encouraged us to apply this model to other systems. Since the electronic structure of graphene is well reproduced by the realistic TB model, we use this model to calculate the SHCs in both undoped and doped (metallic) graphene, and compare the results with those calculated using the Kane-Mele model,[11] which contains only a p_z orbital and an effective SOI to produce an energy gap at the Fermi energy.

In the present Rapid Communication, we adopt a realistic multiorbital (s, p_x, p_y, and p_z orbitals) TB model with the atomic SOI on a honeycomb lattice, and use the Kubo-Streda formula[21] to calculate the SHC. It should be noted that the p_x and p_y orbitals contribute to the SHC because they are mixed with the p_z orbital via the atomic SOI. By calculating the SHC as a function of the Fermi energy, we find that the SHC becomes large in the energy region where the p_x and p_y orbitals are dominant, far away from the Dirac point. The effect of the CVC, which is calculated in the self-consistent Born approximation, is appreciable and causes the SHC to double compared to that without the CVC, while the qualitative behavior of the SHC remains unchanged. In the case of insulating graphene, SHC is not quantized because s_z is not conserved due to the SOI between the p_x (p_y) and p_z orbitals.

The Hamiltonian for electrons on the honeycomb lattice, which is decomposed into A and B sublattices, is given as $\hat{H}=\hat{H}_0+\hat{H}_{\mathrm{SO}}$ where $\hat{H}_0$ and $\hat{H}_{\mathrm{SO}}$ are the kinetic and SOI terms, respectively. $\hat{H}_0$ is given as

$$\hat{H}_0=\sum_{i\subset \mathrm{A(B)}}\sum_{j\subset \mathrm{B(A)}}\sum_{\alpha\beta\sigma} t_{ij}^{\alpha\beta} c_{i\sigma}^{\alpha\dagger} c_{j\sigma}^{\beta}, \tag{1}$$

where $t_{ij}^{\alpha\beta}$ denotes the nearest-neighbor hopping integral between the α orbital at site i and the β orbital at site j, and σ denotes the spin. The Slater-Koster parameters in the TB model are taken as $ss\sigma=-0.86$, $sp\sigma=1.14$, $pp\sigma=1.0$, and $pp\pi=-0.5$ in units of $pp\sigma(5.7\ \mathrm{eV})$.[22] Hereafter, we take $pp\sigma$ and the lattice constant $a(2.55\ \text{Å})$ as the units for energy and length, respectively. We also put $\hbar=1$.

$\hat{H}_{\mathrm{SO}}$ represents the atomic SOI given as

$$\hat{H}_{\mathrm{SO}}=\lambda\sum_i \boldsymbol{l}_i\cdot\boldsymbol{s}_i, \tag{2}$$

where λ is the interaction constant, and $\boldsymbol{l}$ and $\boldsymbol{s}$ are the orbital and spin angular momentum, respectively. $\hat{H}_{\mathrm{SO}}$ has off-diagonal elements such as $\langle p_x\pm|\hat{H}_{\mathrm{SO}}|p_y\pm\rangle=\mp i\lambda/2$, $\langle p_x\pm|\hat{H}_{\mathrm{SO}}|p_z\mp\rangle=\pm\lambda/2$, and $\langle p_y\pm|\hat{H}_{\mathrm{SO}}|p_z\mp\rangle=-i\lambda/2$, where $|l\sigma\rangle$ represents an electron with orbital l and spin $\sigma=\pm1$.

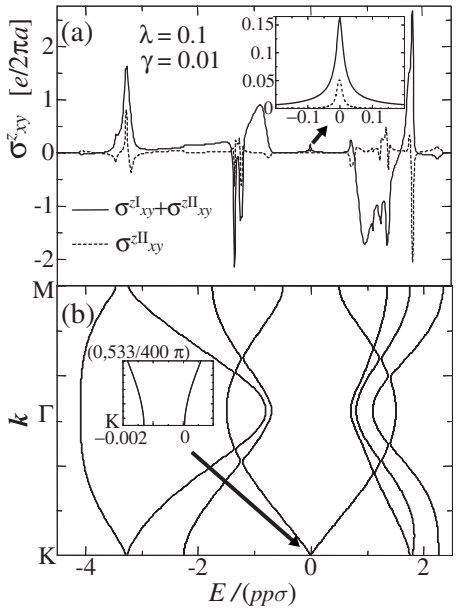

FIG. 1. (a) SHC $\sigma^{z\mathrm{I}}_{xy}+\sigma^{z\mathrm{II}}_{xy}$ (solid line) and $\sigma^{z\mathrm{II}}_{xy}$ (dotted line), and (b) band structure through $\boldsymbol{k}$ points $K=(0,4\pi/3)$, $\Gamma=(0,0)$, and $M=(\pi/\sqrt{3},\pi)$ against energy for atomic SOI $\lambda=0.1$ and damping $\gamma=0.01$ (in units of $pp\sigma$). The insets show the SHC and band structure near the Dirac point.

According to Streda,[21] the intrinsic SHC at $T=0$ is given as $\sigma^{z}_{xy}=\sigma^{z\mathrm{I}}_{xy}+\sigma^{z\mathrm{II}}_{xy}$, where

$$\sigma^{z\mathrm{I}}_{xy}(E)=\frac{1}{2\pi N}\sum_{\boldsymbol{k}}\mathrm{Tr}[\hat{J}^{S}_{x}\hat{G}^{R}\hat{J}^{C}_{y}\hat{G}^{A}]_{\omega=E}, \tag{3}$$

$$\sigma^{z\mathrm{II}}_{xy}(E)=\frac{-1}{4\pi N}\sum_{\boldsymbol{k}}\int_{-\infty}^{E}d\omega \times\mathrm{Tr}\left[\hat{J}^{S}_{x}\frac{\partial\hat{G}^{R}}{\partial\omega}\hat{J}^{C}_{y}\hat{G}^{R}-\hat{J}^{S}_{x}\hat{G}^{R}\hat{J}^{C}_{y}\frac{\partial\hat{G}^{R}}{\partial\omega}-\langle R\leftrightarrow A\rangle\right]. \tag{4}$$

Here, $\hat{G}^{R(A)}$ is the retarded (advanced) Green's function given as $\hat{G}^{R(A)}(\boldsymbol{k},\omega)=[\omega-\hat{H}+(-)i\hat{\Gamma}]^{-1}$, where $\hat{\Gamma}$ is the matrix form of the imaginary part of the self-energy (damping rate) due to scattering by local impurities. The Green's functions are represented by 16×16 matrices in the momentum representation.

The matrix forms of the charge and s_z-spin current operators for the μ direction ($\mu=x,y$) are given by $\hat{J}^{C}_{\mu}=-e\frac{\partial\hat{H}}{\partial k_{\mu}}$ and $\hat{J}^{S}_{\mu}=-\frac{1}{2e}\{\hat{J}^{C}_{\mu},s_z\}$, respectively. In the SHC, $\sigma^{z\mathrm{I}}_{xy}$ and $\sigma^{z\mathrm{II}}_{xy}$ represent the "Fermi-surface term" and the "Fermi-sea term," respectively. In this Rapid Communication, we take $N=900\times900$ $\boldsymbol{k}$-point meshes in the numerical calculations.

We first neglect the CVC and assume that the damping matrix is diagonal and is independent of orbital $\hat{\Gamma}_{\alpha\beta}=\gamma\delta_{\alpha\beta}$. Figures 1(a) and 1(b) give the calculated results of the SHC as a function of the position of the Fermi energy E_F and the band structure of graphene for $\lambda=0.1$ and $\gamma=0.01$ (in units of $pp\sigma$), respectively. In Fig. 1(a), the solid and dotted lines denote σ^{z}_{xy} and $\sigma^{z\mathrm{II}}_{xy}$, respectively. We observe that the SHC σ^{z}_{xy} is large in energy regions where the bands are nearly degenerate, while $\sigma^{z\mathrm{II}}_{xy}$ exhibits peak structures in these energy regions. In the metallic region, the magnitude of $\sigma^{z\mathrm{I}}_{xy}$ is much larger than that of $\sigma^{z\mathrm{II}}_{xy}$.

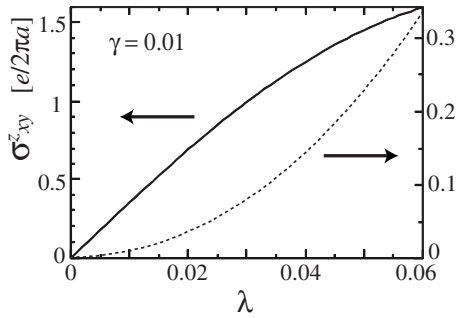

FIG. 2. σ^{z}_{xy} against λ with $\gamma=0.01$ (in units of $pp\sigma$) for $n=3.2$ ($E_F=-1$) (solid line) and for $n=4$ ($E_F=0$) (dotted line), respectively.

The insets of Figs. 1(a) and 1(b) show the SHC and the band structure near the Dirac point of graphene, i.e., $E_F=0$. The Dirac point at K is split by the atomic SOI, and forms an energy gap with $\Delta_D=0.0013$ when $\lambda=0.1$.

In order to study the SHE in graphene, we estimate the value of γ to be about 0.005 by comparing the longitudinal conductivity σ_{xx} calculated in the present model with the experimental resistivity observed for doped graphene $\rho=1/\sigma_{xx}=100\ \Omega$.[23] In this case, the number of electrons n per atom of doped graphene is $n=3.998$, which corresponds to $E_F=-0.05$ in the present model. The value of λ of the atomic SOI at the Dirac point in graphene is estimated to be $\lambda=0.001$,[24,25] which corresponds to an energy gap $\Delta_D=2\times10^{-7}(\sim10^{-6}$ eV). The SHC calculated by using $\lambda=0.001$ and $\gamma=0.005$, and by neglecting the energy dependence of γ, is $\sigma^{z}_{xy}\sim3\times10^{-5}[e/2\pi a]$ at the Dirac point. This value is much smaller than the quantized SHC $e/2\pi a$, since $\gamma\gg\Delta_D$ and the graphene is metallic for these parameter values.

The SHC may increase in doped graphene; for example, the value of σ^{z}_{xy} increases to $\sim0.1[e/2\pi a]$ at $E_F=-0.76$, which can be realized by substituting 50% carbon atoms with boron atoms. Although this situation may be virtual, similar electronic state may be realized by graphite intercalation. Since $1[e/2\pi a]\sim1500(\hbar/e)(\Omega\ \mathrm{cm})^{-1}$ in the present case ($a=2.55$ Å), the SHC $\sim150(\hbar/e)(\Omega\ \mathrm{cm})^{-1}$ at $E_F=-0.76$ is the same order as that of Pt.

Now we give an intuitive explanation of why the SHE is induced by the atomic SOI. The calculated λ dependence of the SHC is shown in Fig. 2. We see that $\sigma^{z}_{xy}\propto\lambda$ and $\sigma^{z}_{xy}\propto\lambda^2$ for $n=3.2$ ($E_F=-1$) and $n=4$ ($E_F=0$), respectively. The results may be interpreted as follows. Since the p_x and p_y orbitals are dominant at $E_F\sim-1$, an anticlockwise motion of an up-spin electron on p_y orbitals in a honeycomb lattice may be given by Fig. 3(a). The arrows in the figure represent an interorbital transition induced by the atomic SOI. In the process $p_y\rightarrow p_x$ ($p_x\rightarrow p_y$), the SOI works once and yields a factor $(-)i\lambda/2$, which is the first order of λ. The corresponding motion of an electron yields a factor $i=e^{2\pi i/4}$, which can be

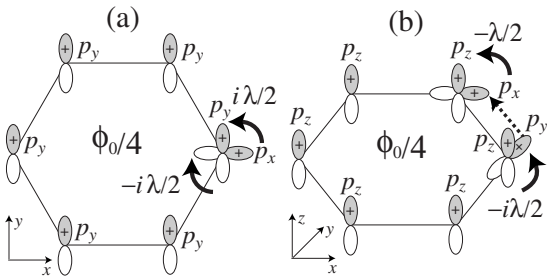

FIG. 3. Effective AB phase in honeycomb lattice derived by a motion of an up-spin electron (a) on mainly p_x and p_y orbitals, and (b) on mainly p_z orbital.

interpreted as the Aharonov-Bohm (AB) phase factor $e^{2\pi i\phi/\phi_0}$ ($\phi_0=hc/|e|$), where ϕ is effective magnetic flux $\phi=\oint \boldsymbol{A}\cdot d\boldsymbol{r}=\phi_0/4$ through a honeycomb lattice. Since the sign of the effective magnetic flux is opposite for down-spin electrons, up- and down-spin electrons move in opposite directions under an electric field. By this process, $\sigma_{xy}^z \propto \lambda$ is realized in the region where the p_x and p_y orbitals are dominant, as indicated by the solid line in Fig. 2.

At $E_F\sim 0$ the p_z orbital is dominant, and an important process of an up-spin electron on p_z orbitals may be given by Fig. 3(b). Solid arrows and a dotted arrow represent the interorbital transitions induced by the SOI and by hopping, respectively. The SOI should operate at least twice while the electron moves around the honeycomb structure, since the spin is flipped in the transitions $p_z\rightarrow p_y$ and $p_x\rightarrow p_z$ via the SOI in this case. The corresponding motion yields a factor of $i=e^{2\pi i/4}$, which corresponds to the AB phase and an effective magnetic flux. By this process, $\sigma_{xy}^z \propto \lambda^2$ is realized in the region where the p_z orbital is dominant at the Fermi level, as indicated by the dotted line in Fig. 2. Since $\lambda \ll 1$, the SHC near $E_F=0$ is about 10 times smaller than that near $E_F=-1$.

Up until now, the CVCs have not been taken into account. However, the CVCs may play an important role for the SHC in graphene, as discussed in Ref. 12 for the Kane-Mele model. In order to study the role of the CVC in the present four-orbital model, we employ the self-consistent Born approximation, where orbital-dependent damping $\hat{\Gamma}_{\alpha\beta}=\gamma_\alpha\delta_{\alpha\beta}$ is given by

$$\gamma_\alpha(E)=n_i I^2\frac{1}{2Ni}\sum_{\boldsymbol{k}}[\hat{G}^A_{\alpha\alpha}(\boldsymbol{k},E)-\hat{G}^R_{\alpha\alpha}(\boldsymbol{k},E)], \tag{5}$$

where n_i and I are the density of impurities and impurity potentials, respectively. The total current ($\tilde{\hat{J}}_y^C=\hat{J}_y^C+\Delta\hat{J}_y^C$) with the CVC ($\Delta\hat{J}_y^C$) is given by the Bethe-Salpeter equation:

$$\tilde{\hat{J}}_y^C(\boldsymbol{k},\omega)=\hat{J}_y^C(\boldsymbol{k})+\frac{n_i I^2}{N}\sum_{\boldsymbol{k}'}\hat{G}^R(\boldsymbol{k}',\omega)\tilde{\hat{J}}_y^C(\boldsymbol{k}',\omega)\hat{G}^A(\boldsymbol{k}',\omega), \tag{6}$$

which is solved self-consistently. Here, we put $n_i I^2=0.02$, for which the experimental value of resistivity[23] $\rho=1/\sigma_{xx}=100\ \Omega$ at $E_F=-0.05$ is realized in the present calculation. The CVC part for the Fermi-surface term is obtained from

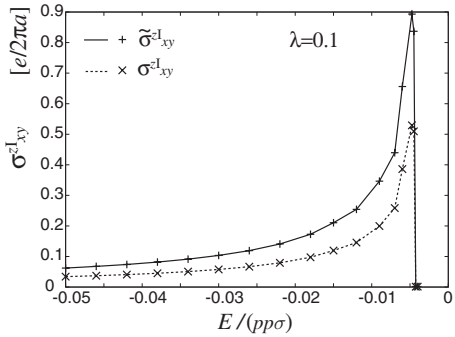

FIG. 4. Total $\tilde{\sigma}_{xy}^{z\mathrm{I}}$ (solid line) with the CVC and $\sigma_{xy}^{z\mathrm{I}}$ (dotted line) without the CVC for $\lambda=0.1$ and $\Delta_D=0.0013$.

$$\Delta\sigma_{xy}^{z\mathrm{I}}(E)=\frac{1}{2\pi N}\sum_{\boldsymbol{k}}\mathrm{Tr}[\hat{J}_x^S\hat{G}^R\Delta\hat{J}_y^C\hat{G}^A]_{\omega=E}, \tag{7}$$

and the total SHC with the CVC is given by $\tilde{\sigma}_{xy}^{z\mathrm{I}}=\sigma_{xy}^{z\mathrm{I}}+\Delta\sigma_{xy}^{z\mathrm{I}}$.

The calculated results of $\sigma_{xy}^{z\mathrm{I}}$ and $\tilde{\sigma}_{xy}^{z\mathrm{I}}$ near the Dirac point are shown in Fig. 4 for $\lambda=0.1$, which makes $\Delta_D=0.0013$ at the Dirac point. The numerical results for $|E|<0.004$ are omitted because of poor convergence. We note that $\tilde{\sigma}_{xy}^{z\mathrm{I}}=0$ in the insulating system ($E_F=0$). We see that $\tilde{\sigma}_{xy}^{z\mathrm{I}}$ with the CVC is almost double $\sigma_{xy}^{z\mathrm{I}}$ without the CVC. Although the behavior of $\sigma_{xy}^{z\mathrm{I}}$ is consistent with the results of Sinitsyn *et al.*,[12] $\tilde{\sigma}_{xy}^{z\mathrm{I}}$ is considerably smaller than that obtained by Sinitsyn *et al.* We consider that the disagreement comes from the difference between two models. The reason why the CVC remains for the atomic SOI in a honeycomb lattice is that the Hamiltonian breaks inversion symmetry $\hat{H}_{\alpha\beta}(\boldsymbol{k})\neq\hat{H}_{\alpha\beta}(-\boldsymbol{k})$. If $\hat{H}_{\alpha\beta}(\boldsymbol{k})=\hat{H}_{\alpha\beta}(-\boldsymbol{k})$ is satisfied, the CVC vanishes identically. We note that the CVC is absent for the Fermi–sea term in the Born approximation in the present model.

In the Kane-Mele model, the SHE $\sigma_{xy}^z=e/2\pi$ is quantized at the Dirac point of graphene.[11] In order to compare with their results, we calculate σ_{xy}^z in the energy gap by taking the limit $\gamma\rightarrow 0$, which corresponds to insulating graphene. We obtain $\sigma_{xy}^{z\mathrm{I}}=0$ and $\sigma_{xy}^{z\mathrm{II}}\sim 1.2e/2\pi$ at $E_F=0$ for $\lambda=0.4$. The reason for the violation of the quantization is that s_z is not conserved due to the SOI in the present model.[26,27]

So far we have neglected the effect of lattice deformation (curvature effect), which was pointed out to be important for, e.g., carbon nanotubes.[25,28,29] The curvature effect induces a hopping (Δt) between the p_z orbital and p_x (p_y) orbital. Δt is estimated as ~ 0.01 in graphene[30] and ~ 0.1 in a nanotube[31] in units of $pp\sigma$. The lowest order of the curvature effect on SHC $\sigma_{xy\ \mathrm{curv}}^z$ is estimated as $(\Delta t)^2\lambda$, where a denominator of order 1 eV is omitted. Since the SHC $\sigma_{xy\ \mathrm{int}}^z$ without the curvature effect is the order of λ^2, the ratio $\sigma_{xy\ \mathrm{curv}}^z/\sigma_{xy\ \mathrm{int}}^z \sim 0.1$ in the graphene, and ~ 10 in the nanotube by adopting a realistic value of $\lambda=0.001$ for the SOI of carbon atoms. We expect that the curvature effect for the SHC may be small in graphene but dominant in the nanotube.

In summary, we have studied the SHC in a two-dimensional honeycomb lattice using a realistic band structure consisting of s, p_x, p_y, and p_z orbitals with the atomic

SOI. The estimated SHC for a realistic value of the atomic spin-orbit coupling λ and constant damping γ for the metallic graphene at the Dirac point is considerably small. We predict that the SHC will be large when the Fermi level is shifted to $E_F=-0.76$ (~ -4.3 eV), where the p_x and p_y orbitals are dominant at the Fermi level. In the self-consistent Born approximation, the SHC $\tilde{\sigma}_{xy}^{z\mathrm{I}}$ with the CVC is almost double the SHC without the CVC. The obtained value of $\tilde{\sigma}_{xy}^{z\mathrm{I}}$ is considerably smaller than that of the Kane-Mele model.[11,12] In the case of insulating graphene, the obtained SHC $\sigma_{xy}^{z\mathrm{II}}$ is not quantized because s_z is not conserved due to the SOI.

This work was supported by a Grant-in-Aid for 21st Century COE "Frontiers of Computational Science" and a Grant-in-Aid for Scientific Research in Priority Areas "Creation and Control of Spin Current." Numerical calculations were performed at the supercomputer center, ISSP.

[1] K. S. Novoselov, A. K. Geim, S. V. Morozov, D. Jiang, Y. Zhang, S. V. Dubonos, I. V. Grigorieva, and A. A. Firsov, Science **306**, 666 (2004).
[2] T. Ando, T. Nakanishi, and R. Saito, J. Phys. Soc. Jpn. **67**, 2857 (1998).
[3] K. S. Novoselov, A. K. Geim, S. V. Morozov, D. Jiang, M. I. Katsuelson, I. V. Grigorieva, S. V. Dubonos, and A. A. Firsov, Nature (London) **438**, 197 (2005).
[4] Y. Zhang, Yan-Wen Tan, Horst L. Stormer, and P. Kim, Nature (London) **438**, 201 (2005).
[5] V. P. Gusynin and S. G. Sharapov, Phys. Rev. Lett. **95**, 146801 (2005).
[6] D. A. Abanin, P. A. Lee, and L. S. Levitov, Phys. Rev. Lett. **96**, 176803 (2006).
[7] K. Nomura and A. H. MacDonald, Phys. Rev. Lett. **96**, 256602 (2006).
[8] D. N. Sheng, L. Sheng, and Z. Y. Weng, Phys. Rev. B **73**, 233406 (2006).
[9] M. Ezawa, J. Phys. Soc. Jpn. **76**, 094701 (2007); Phys. Lett. A **372**, 924 (2008); Physica E (Amsterdam) **40**, 269 (2007).
[10] Y. Hatsugai, T. Fukui, and H. Aoki, Phys. Rev. B **74**, 205414 (2006).
[11] C. L. Kane and E. J. Mele, Phys. Rev. Lett. **95**, 146802 (2005); **95**, 226801 (2005).
[12] N. A. Sinitsyn, J. E. Hill, H. Min, J. Sinova, and A. H. MacDonald, Phys. Rev. Lett. **97**, 106804 (2006).
[13] S. Murakami, N. Nagaosa, and S. C. Zhang, Science **301**, 1348 (2003).
[14] J. Sinova, D. Culcer, Q. Niu, N. A. Sinitsyn, T. Jungwirth, and A. H. MacDonald, Phys. Rev. Lett. **92**, 126603 (2004).
[15] S. O. Valenzuela and M. Tinkham, Nature (London) **442**, 176 (2006).
[16] T. Kimura, Y. Otani, T. Sato, S. Takahashi, and S. Maekawa, Phys. Rev. Lett. **98**, 156601 (2007).
[17] H. Kontani, T. Tanaka, D. S. Hirashima, K. Yamada, and J. Inoue, Phys. Rev. Lett. **100**, 096601 (2008).
[18] H. Kontani, M. Naito, D. S. Hirashima, K. Yamada, and J. Inoue, J. Phys. Soc. Jpn. **76**, 103702 (2007).
[19] T. Tanaka, H. Kontani, M. Naito, T. Naito, D. S. Hirashima, K. Yamada, and J. Inoue, Phys. Rev. B **77**, 165117 (2008).
[20] J. I. Inoue, G. E. W. Bauer, and L. W. Molenkamp, Phys. Rev. B **70**, 041303(R) (2004).
[21] P. Streda, J. Phys. C **15**, L717 (1982).
[22] W. A. Harrison, *Electronic Structure and the Properties of Solids* (Dover, New York, 1989).
[23] Y. Zhang and J. Callaway, Phys. Rev. B **39**, 9397 (1989).
[24] H. Min, J. E. Hill, N. A. Sinitsyn, B. R. Sahu, L. Kleinman, and A. H. MacDonald, Phys. Rev. B **74**, 165310 (2006).
[25] D. Huertas-Hernando, F. Guinea, and A. Brataas, Phys. Rev. B **74**, 155426 (2006).
[26] S. Murakami, Phys. Rev. Lett. **97**, 236805 (2006).
[27] L. Sheng, D. N. Sheng, C. S. Ting, and F. D. M. Haldane, Phys. Rev. Lett. **95**, 136602 (2005).
[28] T. Ando, J. Phys. Soc. Jpn. **69**, 1757 (2000).
[29] D. V. Bulaev, B. Trauzettel, and D. Loss, Phys. Rev. B **77**, 235301 (2008).
[30] S. V. Morozov, K. S. Novoselov, M. I. Katsnelson, F. Schedin, L. A. Ponomarenko, D. Jiang, and A. K. Geim, Phys. Rev. Lett. **97**, 016801 (2006).
[31] F. Kuemmeth, S. Ilani, D. C. Ralph, and P. L. McEuen, Nature (London) **452**, 448 (2008).